PERGAMON

Journal of Structural Geology 21 (1999) 597–611

JOURNAL OF STRUCTURAL GEOLOGY

A stress inversion procedure for polyphase calcite twin and fault/slip data sets

Michal Nemcok[a,*,1], Dušan Kovác[b], Richard J. Lisle[c]

[a]*Institute for Geology and Palaeontology, University of Salzburg, Hellbrunner strasse 34, 5010 Salzburg, Austria*
[b]*ADEC Software and Hardware, Jaskový Rad 173, 831 01 Bratislava, Slovak Republic*
[c]*Laboratory for Strain Analysis, Department of Earth Sciences, University of Wales, Cardiff CF1 3YE, UK*

Received 27 November 1997; accepted 22 February 1999

Abstract

In rocks that are polydeformed an approach which separates faults prior to stress inversion is more appropriate. The traditional stress inversion approach involving the concept of the *best-fit stress tensor*, e.g. a tensor which minimises the misfit between calculated and measured fault-striae data, often risks computing artificial stress tensors that are some form of average of mixed sets of real stress tensors. A new approach is proposed in which fault data are pre-processed to group the faults on the basis of their response to all possible orientations and magnitudes of applied stress. A computer method is described which utilises cluster analysis based on the *right-dihedra method* to divide dynamically-mixed fault populations to monophase subsets. This division is based on the ranked similarity coefficients of each fault pair from the raw data set. The data clusters form dynamically-homogeneous subsets, which are used for the composite right-dihedra solution. This solution is re-computed for the reduced stress tensor defined by the orientation of principal stress axes and the ratio of their magnitudes.

1. Introduction

Calcite twin and fault-striae data have been widely analysed in structural studies since Weiss (1954) and Turner (1953, 1962) developed techniques to determine stress axes from calcite *e*-lamellae (e.g. Rose, 1868; Mügge, 1883) (Fig. 1) and Carey and Brunier (1974) devised a method to compute the *reduced stress tensor* (sensu Angelier, 1989), based on the stress–slip relationship (Wallace, 1951; Bott, 1959).

Several of these techniques have been devised for paleostress determination from calcite twin data from unmetamorphosed, macroscopically undeformed or very weakly deformed cover rocks (e.g. Turner, 1962; Nissen, 1964; Spang, 1972; Laurent et al., 1981, 1990; Dietrich and Song, 1984; Pfiffner and Burkhard, 1987; Lacombe and Laurent, 1996). The usual assumptions are: (1) twinning in calcite is a deformation mechanism with no temperature, normal stress and fluid pressure dependence; (2) the yield shear stress value for twinning is a constant; and (3) the stress at the grain scale is homogeneous. Wenk et al. (1983), Burkhard (1993) and Lacombe and Laurent (1996) discussed the validity of these assumptions. Several of these techniques are applied for paleostress analysis in brittle tectonic environments from measurements of faults and their slip vectors (e.g. Angelier, 1979, 1984, 1990, 1994; Etchecopar et al., 1981; Armijo et al., 1982; Gephart and Forsyth, 1984; Michael, 1984; Reches, 1987; Gephart, 1990; Hardcastle and Hills, 1991). The majority of these methods are based on the following assumptions:

1. Fault slip recorded by the striation or other linear structures on the fault plane is parallel to the direction of resolved shear stress on the fault.

* Corresponding author.
E-mail address: mnemcok@egi.utah.edu (M. Nemcok)
[1] Present address: Energy and Geoscience Institute, University of Utah, 423 Wakara Way, Salt Lake City, UT 84108, USA.

0191-8141/99/$ - see front matter
PII: S0191-8141(99)00053-X

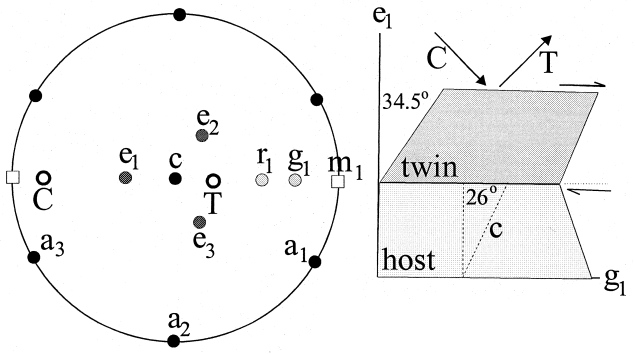

Fig. 1. Geometry of calcite *e*-twinning (after Burkhard, 1993). Equal area projection indicates a position of the principal axes (c, a_1, a_2, a_3) of calcite and a selection of poles of important crystallographic planes: twin plane poles e_1, e_2 and e_3, glide direction g_1, rhombohedral plane pole r_1 and prismatic plane pole m_1. Optimum compression C and tension T axes for twinning on e_1 twin plane are indicated. The section through C, e_1, c, T, r_1 and g_1 in the equal area projection is shown as the schematic representation of an *e*-twin indicated in e_1–g_1 cross-section through host and twin. The section shows the angular relationships between the major crystallographic elements and the optimum compression C and tension T for twinning on e_1. Shear strain for an individual twin is $\gamma = \tan 34.5^\circ$ and c-axis is at angle 26° from the e_1.

2. Slip on each fault plane is independent of slip on other fault planes.
3. The controlling stresses are homogeneous.

The validity of these basic assumptions is discussed in detail by Dupin et al. (1993) and Pollard et al. (1993).

The assumption of stress homogeneity is critical because the existence of polyphase fault reactivation and polyphase twin data sets is common. If such data are analysed by standard paleostress techniques, the results can form spurious compromise values among the different actual stress tensors represented in the data. Under such circumstances, which were numerically tested on synthetically generated faults by Nemcok and Lisle (1995), the control of the polyphase data separation can be lost and the search for the ideal stress tensor leads to the determination of the first spurious compromise tensor. This tensor is used as a criterion for the separation of the first monophase data set from the whole data set. The remaining data are used for further separations. The separation of the polyphase calcite twin data is even more complicated, because the relationship between displacement and stress is looser, partly controlled by crystallography (e.g. Burkhard, 1993).

This paper addresses the issue of analysing polyphase data sets and proposes a new separation/stress inversion computer approach. In order to design this method to apply also to the calcite twin data, the less limited right dihedra constraint for fitting stresses to faults is applied. The presented approach separates faults prior to stress inversion on the basis of their response to all possible orientations and magnitudes of applied stress. Final right-dihedra solutions are recomputed to *reduced stress tensors* defined by the orientation of principal stress axes and the ratio of principal stress difference.

2. Existing methods for polyphase data sets

The development of geological structures is often a complex process in which stresses varied through time. In such cases, various stress states are recorded in polyphase and reactivated fault systems. The traditional stress inversion approach (e.g. Etchecopar et al., 1981; Armijo et al., 1982; Angelier, 1984; Gephart and Forsyth, 1984; Michael, 1984; Galindo-Zaldivar and Gonzales-Lodeiro, 1988; Gephart, 1990; Hardcastle and Hills, 1991) involves the concept of the *best-fit stress tensor*. This is the tensor which best explains the striation data, by minimising the misfit between calculated and measured fault-striae orientation. Testing of this approach using performance sensitivity software written by Nemcok and Lisle (1995) with various combinations of synthetic faults shows that this approach is suitable only for monophase data sets with few spurious measurements. It is not suited to truly mixed data sets because in these circumstances the best-fit tensor risks being a statistical artefact without structural significance. Attempts to improve the solution by a process of rejecting spurious data to improve the best-fit tensor only increases the risk of artificial results.

A similar drawback is associated with the established procedures for polyphase calcite-twin data. The methods of Laurent et al. (1981, 1990), Laurent (1984) and Etchecopar (1984) find the stress tensor that best fits the distribution of the twinned and the untwinned planes measured in a sample. This procedure leads to the stress tensor solution which accounts for the largest number of twinned planes and simultaneously corresponds to the smallest value of f:

$$f = \sum_{j=1}^{N} (\tau_{sj} - \tau_{a'}), \tag{1}$$

where $\tau_{a'}$ is the smallest resolved shear stress applied on the twinned planes compatible with the tensor and τ_{sj}, the resolved shear stress applied on the untwinned planes, for which $\tau_{sj} > \tau_{a'}$. Inconsistent twin data are withdrawn and either considered to be outliers suitable only for rejection or the computing procedure is repeated with them. In order to treat incompatible twin sets which obscure any least square analysis (e.g. Will and Powell, 1991), Laurent et al. (1990), for example, reject up to 20% of incompatible twins rather

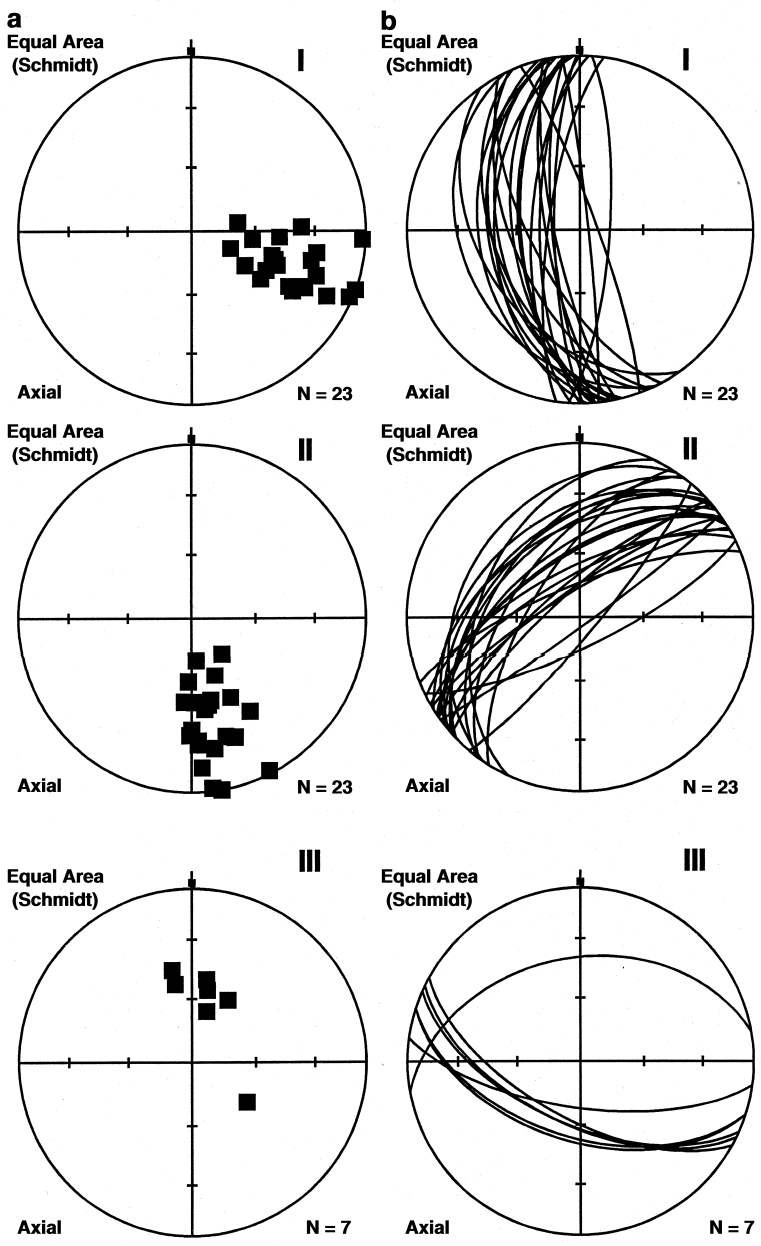

Fig. 2. Three numerically generated calcite twin data sets I, II and III with (a) *c*-axes and (b) e_1 twin planes indicated in equal area projection. Sets I, II and III were used for calculation of the polyphase fault-striae data set in Table 1 (fault Nos. 1–23, 24–46 and 47–53). The sense of twinning is indicated in Table 1.

than utilise them for the determination of superposed stress tensors.

In rocks that are polydeformed an approach that separates faults prior to stress inversion is more appropriate. Several methods have been proposed (e.g. Angelier and Manoussis, 1980; Simón-Gómez, 1986; Huang, 1988; Kleinspehn et al., 1989), but each of them functions only in a very limited number of cases (see the discussion in Nemcok and Lisle, 1995).

Nemcok and Lisle (1995) propose a way of separating fault-striae data, which involves the statistical classification by cluster analysis. The method can be used on randomly oriented reactivated faults. Using a modified numeric method of Hardcastle and Hills (1991), their method assigns to each fault a wide range of potential stress tensors which could have created or reactivated the fault. The faults are compared on the basis of the tensors that succeed or fail to activate/reactivate the fault. Cluster analysis is used to establish degrees of similarity of the faults based on their response to the multiple stress tensors. Separated fault sets can be analysed by any inversion method for monophase data.

The computer method that we present in this paper

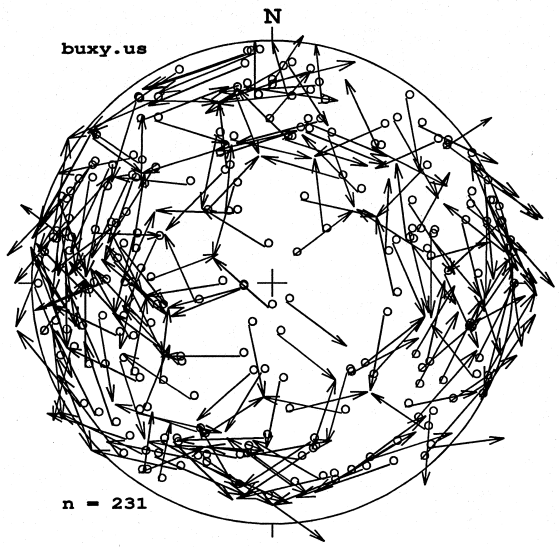

Fig. 3. Experimentally generated calcite twin data set *Buxy 00*, provided by Laurent. *e*-Plane poles (circles) and *c*-axes within the untwinned part of the crystal (end of arrows) are plotted in equal area projection according to the method of Dietrich and Song (1984) by software EC-PLOT of Sperner and Ratschbacher (1994). Glide directions for the *e*-twins are indicated by arrows, which point away from the maximum compressive stress σ_1.

involves cluster analysis combined with the *right-dihedra method* (Angelier and Mechler, 1977). The right-dihedra method constrains the orientation of the principal stresses in the cluster analysis. The use of the less limited constraint of placing the stress axes in dihedra (three-dimensional quadrants) permits slip to occur in directions other than those of the maximum shear stress. Thus, this approach accommodates calcite twin data, but is also suitable for analysis of fault-striae polyphase data. In the case of calcite twin data, the method maps all probable stress states without a need for using non-slip twin data, which is a requirement of numeric stress inversion methods.

3. The new approach

Our method for stress analysis is performed in a number of steps:

1. Each fault-striae measurement is assigned by a right-dihedra graphical stress solution, a three-dimensional representation of all potential stress tensors that could activate/reactivate the fault. Representative *capable* and *non-capable* stress tensors are extracted from the right-dihedra.
2. A *similarity coefficients matrix* is created to quantify degrees of similarity of the faults based on their response to multiple stress tensors.
3. Cluster analysis is used to group the faults based on response to the multiple stress tensors.

Table 1
Fault-striae data *3mixtest* file used for the method testing. F—fault, F. plane—fault plane, Dip dir—dip direction, Tr—trend, Pl—plunge, Displ. sense—displacement sense

F. No.	F. plane		Striae		Displ. sense
	Dip dir	Dip	Tr	Pl	
01	084	86	174	09	dextral
02	094	76	173	39	dextral
03	070	82	157	24	dextral
04	258	78	177	39	dextral
05	278	75	203	42	dextral
06	269	78	180	08	dextral
07	270	71	187	22	dextral
08	260	74	182	36	dextral
09	242	67	168	34	dextral
10	273	67	199	33	dextral
11	261	41	205	25	dextral
12	258	51	186	25	dextral
13	244	32	190	18	dextral
14	235	42	187	32	dextral
15	260	46	189	21	dextral
16	265	77	182	29	dextral
17	246	58	183	41	dextral
18	266	62	182	11	dextral
19	256	48	185	21	dextral
20	268	49	202	28	dextral
21	262	58	199	33	dextral
22	265	61	211	36	dextral
23	247	49	202	25	dextral
24	144	86	232	22	dextral
25	154	76	238	20	dextral
26	130	82	217	17	dextral
27	318	78	234	28	dextral
28	338	75	275	60	dextral
29	329	78	246	31	dextral
30	330	71	253	34	dextral
31	320	74	239	29	dextral
32	302	67	229	34	dextral
33	333	67	265	41	dextral
34	321	41	256	20	dextral
35	318	51	251	26	dextral
36	304	32	243	17	dextral
37	295	42	243	29	dextral
38	320	46	255	23	dextral
39	325	77	242	29	dextral
40	306	58	238	31	dextral
41	326	62	254	30	dextral
42	316	48	250	25	dextral
43	328	49	273	33	dextral
44	322	58	252	28	dextral
45	325	61	253	30	dextral
46	307	49	244	28	dextral
47	204	60	234	54	normal
48	206	60	196	59	normal
49	198	54	256	34	normal
50	209	63	258	48	normal
51	198	52	202	50	normal
52	350	40	054	17	normal
53	188	68	245	52	normal

Table 2
Calcite twin data from experimentally deformed Jurassic limestone from locality Buxy in Burgundy, France, provided by Laurent (personal communication, 1998). Triaxial deformation was made at 200°C. Most of the deformation (up to 10%) was achieved by twinning on the *e*-planes. The limestone did not indicate any macroscopic deformation. Thin sections indicate up to 0.5% of the twinning as a result of the natural deformation (Laurent, 1998, personal communication). Applied stress, that created experimental twin data, had principal directions $\sigma_1 = 204/87$, $\sigma_2 = 317/01$, $\sigma_3 = 047/02$, stress ratio $\varphi = 0.07$ (sensu Etchecopar et al., 1981) and σ_1–σ_3 magnitude was equal to 173 MPa. *c*—*c*-axes, *e*—twin planes, *a*—angles between *c*-axes and twin plane poles. The data are represented by the Turbo Pascal software TWIN of Sperner and Ratschbacher (1994), using a convention where U-stage contains the vertical N axis with zero in S and clockwise counting, the horizontal north-trending *H* axis and the horizontal east-trending axis. Whereas reading of N is independent of the orientation of the measured axis or pole, the record of the *H* and *K* axes is orientation-dependent. For *c*-axis or plane pole parallel to the *K*-axis (i.e. horizontal E–W, $K = 0$), *H* values are counted from the vertical towards the thin section plane with tilting towards the W being positive and towards the E being negative. Due to inaccuracies in U-stage handling, planes are identified as *e*-twins ($a = 26°$) and used for later test-paleostress calculation for $16° < a < 35°$

c			e_1		a_1	e_2		a_2	e_3		a_3
N	*H*	*K*	*N*	*H*		*N*	*H*		*N*	*H*	
318	35	0	306	8	27						
268	62	0	283	76	20	274	35	27	240	70	27
33	88	0	7	89	26						
232	75	0	259	66	27	208	61	26			
263	82	0	237	79	26	91	73	26	282	64	26
313	61	0	159	44	79						
178	82	0	160	60	28	347	72	28			
66	76	0	231	72	35	53	62	18			
172	60	0	193	40	25	143	62	25			
186	87	0	346	73	28	180	60	28			
156	22	0	111	37	26	179	43	24	262	9	26
260	85	0	286	76	27	75	69	26	239	69	26
270	86	0	249	70	26	85	68	26	295	78	26
199	38	0	172	56	26	192	11	27			
47	63	0	18	49	28	79	60	28			
342	57	0	308	42	30						
145	68	0	130	46	25						
147	48	0	181	53	27	118	28	26			
126	81	0	143	58	28	98	83	28	319	76	26
319	89	0	297	75	26	137	65	26			
47	59	0	15	40	30	78	56	26			
218	73	0	192	63	26	244	61	27	39	81	26
7	89	0	346	72	27	181	65	27			
101	75	0	84	52	27	129	78	27	268	83	25
274	85	0	250	73	26	95	69	26			
343	90	0	2	73	25						
80	56	0	113	50	27	48	44	27			
342	79	0	315	73	27	168	76	26	3	61	27
34	79	0	199	78	27	20	54	28			
262	78	0	283	60	27	236	72	26			
192	57	0	161	51	26	220	43	25			
190	53	0	159	43	25	222	44	25			
164	82	0	10	90	27	325	79	27			
319	75	0	291	77	27						
29	73	0	55	61	27						

Table 2 (*continued*)

c			e_1		a_1	e_2		a_2	e_3		a_3
N	*H*	*K*	*N*	*H*		*N*	*H*		*N*	*H*	
116	85	0	94	99	22						
253	58	0	275	77	28	225	69	27	263	32	27
196	70	0	223	80	28	175	89	28			
352	67	0	323	64	27	17	50	27			
248	65	0	236	90	27	278	66	27			
321	90	0	114	90	27						
80	81	0	92	59	25						
108	69	0	88	81	23						
288	62	0	261	65	24	309	41	26			
242	57	0	260	79	28	257	33	26			
208	81	0	48	80	28	181	89	28			
174	65	0	143	64	28	200	46	28			
108	70	0	80	72	27						
348	56	0	316	43	27	21	51	27			
226	87	0	247	72	25						
174	66	0	202	54	27						
111	52	0	81	56	24						
132	36	0	110	57	26	101	13	26			
179	78	0	152	82	27	16	80	28			
186	44	0	214	60	27	160	62	27	181	18	26
194	37	0	223	54	26	166	55	27	189	11	26
145	71	0	312	86	26						
11	81	0	214	86	26	169	84	27	9	55	26
173	89	0	147	80	27	194	72	27			
241	68	0	267	57	25						
350	87	0	194	79	28	146	80	27			
227	62	0	237	88	28						
188	83	0	218	83	30						
178	80	0	335	87	26	21	86	27			
38	67	0	55	87	26						
356	76	0	328	71	27	17	58	26			
44	85	0	244	79	26	200	85	26			
43	38	0	70	57	27	12	54	27	54	12	26
159	89	0	309	88	30						
175	78	0	330	89	28	19	88	28			
314	77	0	286	79	27						
351	78	0	18	72	27	328	61	27			
1	81	0	26	88	26	163	79	27			
199	87	0	230	88	31						
106	52	0	125	74	28	75	61	27	124	29	26
139	61	0	110	52	26	167	50	25	140	87	26
106	74	0	78	76	27						
71	61	0	86	83	26						
332	89	0	359	89	27	316	66	28	138	69	26
355	78	0	156	83	27	21	85	27			
199	79	0	173	87	27	40	83	28			
311	52	0	276	47	27	315	79	27	343	40	26
279	83	0	306	75	28						
177	66	0	158	86	27	205	75	28			
252	90	0	91	75	24						
280	83	0	302	82	22	261	62	28			
346	57	0	334	82	27	18	59	27			
106	70	0	81	81	27	126	87	26	111	44	26
1	66	0	31	56	28	331	56	28			
173	75	0	144	73	28	194	55	27			
182	87	0	338	80	27	25	79	27			
179	75	0	207	69	27	155	58	28			
27	67	0	54	75	27	8	87	27			
125	89	0	97	89	28						
195	76	0	34	88	25						

(*continued on next page*)

Table 2 (*continued*)

c			e_1		a_1	e_2		a_2	e_3		a_3
N	*H*	*K*	*N*	*H*		*N*	*H*		*N*	*H*	
266	41	0	246	62	26	297	53	25	242	17	26
170	90	0	140	89	30	183	67	26			
96	46	0	101	73	27	58	44	27	133	34	26
31	80	0	228	80	26						
167	60	0	136	59	27	192	42	26			
50	54	0	85	52	28	42	80	27			
33	43	0	354	42	26	38	69	26	72	31	26
205	59	0	236	51	26	175	47	27			
215	46	0	226	66	22	181	50	25	247	28	26
155	41	0	114	43	27	164	67	27	195	27	26
146	70	0	169	82	25	126	86	25			
178	71	0	15	87	28	150	77	28			
3	61	0	331	62	28	15	86	27			
70	72	0	98	74	27						
122	88	0	96	89	26						
235	62	0	241	88	27						
179	67	0	150	70	27	193	90	26			
72	47	0	56	70	27	106	54	27	46	25	26
302	41	0	283	63	26	275	18	26			
198	79	0	217	60	26	172	76	26			
347	55	0	315	48	26	19	44	26			
194	73	0	167	79	27	30	86	26			
324	84	0	122	82	26	167	83	26			
186	81	0	158	83	28	22	76	28	199	58	26
33	85	0	234	81	25	191	83	25			
351	89	0	140	90	31						

4. Each resultant subset is tested by the composite right-dihedra solution to establish whether the data belong to a monophase solution. Polyphase sets are divided into monophase subsets at the higher similarity limit.
5. The composite right-dihedra solution of each monophase fault-striae set is recalculated to the *reduced stress tensor* defined by the orientations of principal stress axes and the ratio of their magnitudes.

A detailed description of the procedures is described below.

3.1. Input data

Our procedure requires that the calcite twin data extracted from thin sections with a Universal-stage (Figs. 2 and 3) have to be converted to the fault-striae format, slip direction in a slip plane. This can be done by plotting *c*-axis and *e*-plane with its normal on the stereonet (Fig. 1). The slip vector is found by the intersection of the *e*-plane with the plane comprising *c*-axis and *e*-plane normal. The sense is given by the twinning sense or by the position of the *c*-axis in the extension quadrant. Fault-striae measurements are coded numerically for ease of later separation and comparison. Each measurement is defined by the dip direction and

Table 3
Fault-striae data recalculated from calcite twin data from location Buxy (Table 2). DDr—dip direction, Dp—dip, Tr—trend, Pl—plunge. Relation—relationship indicates related twin planes (twin set 1, 2, 3—planes e_1, e_2, e_3)

Fault		Striation			Relation
DDr	Dp	Tr	Pl	Sen	
324	8	309	8	−1	
347	76	271	46	+1	twin set 1
356	35	10	35	−1	twin set 2
30	70	112	21	+1	twin set 3
263	89	353	3	+1	
11	66	95	13	−1	twin set 1
62	61	346	24	−1	twin set 2
33	79	304	4	−1	twin set 1
179	73	228	65	−1	twin set 2
348	64	56	36	−1	twin set 3
110	60	50	41	−1	twin set 1
283	72	228	61	−1	twin set 2
217	62	153	40	−1	
77	40	131	27	−1	twin set 1
127	62	211	10	+1	twin set 2
284	73	209	41	−1	twin set 1
90	60	65	57	−1	twin set 2
159	37	203	29	+1	twin set 1
91	43	63	39	+1	twin set 2
8	9	312	5	+1	twin set 3
344	76	70	16	−1	twin set 1
195	69	165	67	−1	twin set 2
31	69	315	33	−1	twin set 3
21	70	305	33	−1	twin set 1
185	68	157	66	−1	twin set 2
335	78	62	15	−1	twin set 3
98	56	153	40	+1	twin set 1
78	11	68	11	−1	twin set 2
252	49	177	16	−1	twin set 1
191	60	102	2	+1	twin set 2
322	42	246	12	−1	
140	46	95	37	−1	
89	53	12	17	+1	twin set 1
152	28	94	16	−1	twin set 2
127	58	183	42	−1	twin set 1
172	83	261	6	+1	twin set 2
311	76	19	57	−1	twin set 3
333	75	252	30	−1	twin set 1
133	65	122	65	−1	twin set 2
255	40	186	17	−1	twin set 1
192	56	103	2	+1	twin set 2
78	63	356	15	−1	twin set 1
26	61	105	18	−1	twin set 2
231	81	245	81	−1	twin set 3
284	72	208	35	−1	twin set 1
89	65	60	61	−1	twin set 2
186	52	134	39	−1	twin set 1
141	78	53	9	+1	twin set 2
2	83	283	59	−1	twin set 3
20	73	297	23	−1	twin set 1
175	69	181	69	−1	twin set 2
268	73	344	38	−1	
157	50	245	2	−1	twin set 1
222	44	143	10	−1	twin set 2
315	73	228	9	−1	twin set 1

(*continued on next page*)

Table 3 (*continued*)

Fault		Striation			Relation
DDr	Dp	Tr	Pl	Sen	
102	76	147	70	−1	twin set 2
267	61	336	33	−1	twin set 3
71	78	358	55	−1	twin set 1
250	54	205	44	−1	twin set 2
347	60	55	32	−1	twin set 1
34	72	307	9	−1	twin set 2
109	51	22	3	−1	twin set 1
50	43	123	16	−1	twin set 2
111	43	30	8	−1	twin set 1
48	44	132	7	−1	twin set 2
260	89	350	20	−1	twin set 1
305	79	226	43	−1	twin set 2
339	77	67	7	+1	
215	61	294	18	−1	
176	89	265	11	+1	
355	77	278	45	+1	twin set 1
45	69	123	27	+1	twin set 2
7	32	29	30	−1	twin set 3
47	80	321	24	+1	twin set 1
95	89	184	44	+1	twin set 2
307	64	38	1	+1	twin set 1
253	50	322	24	−1	twin set 2
34	89	123	65	+1	twin set 1
352	66	266	8	+1	twin set 2
156	89	66	2	−1	
178	59	225	48	−1	
182	81	266	34	+1	
9	65	93	12	+1	twin set 1
321	41	14	28	−1	twin set 2
10	79	295	55	+1	twin set 1
13	33	47	28	−1	twin set 2
222	80	302	42	−1	twin set 1
89	89	179	17	+1	twin set 2
127	64	215	4	+1	twin set 1
70	46	136	24	−1	twin set 2
190	72	278	9	+1	
314	43	236	12	−1	twin set 1
249	51	339	1	−1	twin set 2
23	72	102	32	−1	
68	54	147	15	−1	
189	56	268	15	+1	
160	57	207	46	+1	twin set 1
169	13	124	9	−1	twin set 2
118	82	207	11	+1	twin set 1
254	80	331	51	−1	twin set 2
56	60	352	37	+1	twin set 1
110	62	172	41	+1	twin set 2
89	18	81	18	−1	twin set 3
47	54	352	37	+1	twin set 1
104	55	159	40	+1	twin set 2
81	11	74	11	−1	twin set 3
318	86	235	61	−1	
56	86	144	30	−1	twin set 1
101	84	16	34	−1	twin set 2
261	55	253	55	−1	twin set 3
123	80	36	17	−1	twin set 1
76	72	152	35	−1	twin set 2
3	57	83	16	−1	
76	79	160	28	−1	twin set 1
124	80	39	27	−1	twin set 2

Table 3 (*continued*)

Fault		Striation			Relation
DDr	Dp	Tr	Pl	Sen	
33	88	308	71	+1	
52	83	322	2	+1	
295	87	206	30	−1	twin set 1
249	86	336	31	−1	twin set 2
215	87	129	52	+1	
302	71	214	6	−1	twin set 1
253	58	321	32	−1	twin set 2
26	79	107	37	−1	twin set 1
70	85	342	22	−1	twin set 2
200	57	145	41	+1	twin set 1
258	54	317	35	+1	twin set 2
216	12	232	12	−1	twin set 3
321	88	231	5	−1	
300	89	211	28	−1	twin set 1
251	88	339	31	−1	twin set 2
344	79	72	7	+1	
252	72	339	9	−1	twin set 1
302	61	230	29	−1	twin set 2
244	88	154	17	+1	twin set 1
107	79	29	46	−1	twin set 2
40	88	310	2	+1	
145	74	77	53	+1	twin set 1
195	61	271	24	+1	twin set 2
146	29	184	23	−1	twin set 3
160	52	78	9	−1	twin set 1
103	50	182	13	−1	twin set 2
130	87	97	86	+1	twin set 3
192	76	280	8	+1	
184	83	106	58	+1	
271	89	181	1	+1	twin set 1
314	66	253	47	−1	twin set 2
132	69	70	51	−1	twin set 3
114	83	31	45	−1	twin set 1
249	85	160	17	+1	twin set 2
97	87	186	19	+1	twin set 1
230	83	314	40	−1	twin set 2
354	47	83	1	+1	twin set 1
315	79	283	77	+1	twin set 2
287	40	5	10	−1	twin set 3
324	75	50	13	−1	
112	86	197	49	+1	twin set 1
65	75	341	22	+1	twin set 2
179	75	258	35	−1	
328	82	58	1	−1	twin set 1
9	62	305	39	−1	twin set 2
296	82	6	66	+1	twin set 1
252	59	169	11	+1	twin set 2
189	81	275	27	+1	twin set 1
144	87	57	43	+1	twin set 2
159	44	174	43	−1	twin set 3
239	56	322	11	−1	twin set 1
299	56	216	11	−1	twin set 2
126	73	216	1	+1	twin set 1
76	55	140	33	−1	twin set 2
292	80	207	27	−1	twin set 1
245	79	328	30	−1	twin set 2
63	69	150	8	−1	twin set 1
115	58	44	27	−1	twin set 2
216	75	132	21	+1	twin set 1
262	87	348	49	+1	twin set 2

(continued on next page)

Table 3 (*continued*)

Fault		Striation			Relation
DDr	Dp	Tr	Pl	Sen	
173	89	263	1	+1	
236	88	324	41	−1	
24	62	76	49	+1	twin set 1
333	53	269	29	+1	twin set 2
28	17	350	14	−1	twin set 3
130	89	40	2	−1	twin set 1
87	67	144	53	−1	twin set 2
169	73	144	71	+1	twin set 1
212	44	295	7	+1	twin set 2
137	34	218	7	−1	twin set 3
42	80	121	48	−1	
134	59	221	5	+1	twin set 1
78	42	141	22	−1	twin set 2
185	52	99	5	+1	twin set 1
228	80	284	73	+1	twin set 2
276	42	357	8	+1	twin set 1
232	69	212	67	+1	twin set 2
198	31	279	5	−1	twin set 3
34	51	119	7	−1	twin set 1
95	47	17	12	−1	twin set 2
44	66	360	58	+1	twin set 1
89	50	165	15	+1	twin set 2
23	28	87	13	−1	twin set 3
156	43	231	13	+1	twin set 1
106	67	75	64	+1	twin set 2
75	27	152	6	−1	twin set 3
101	82	16	30	+1	twin set 1
144	86	230	41	+1	twin set 2
255	87	340	53	−1	twin set 1
120	77	207	16	+1	twin set 2
299	62	24	9	+1	twin set 1
255	86	175	66	+1	twin set 2
172	74	84	8	+1	
174	89	264	3	+1	
29	88	307	78	+1	
120	70	206	11	+1	twin set 1
77	89	348	59	+1	twin set 2
214	70	270	57	+1	twin set 1
164	54	90	20	+1	twin set 2
224	25	175	17	−1	twin set 3
347	63	37	51	+1	twin set 1
355	18	311	13	−1	twin set 2
53	60	118	36	−1	twin set 1
98	76	9	4	−1	twin set 2
315	48	229	4	−1	twin set 1
251	44	332	9	−1	twin set 2
103	79	190	16	+1	twin set 1
240	86	325	53	−1	twin set 2
148	82	63	32	−1	twin set 1
103	83	190	29	−1	twin set 2
112	83	201	6	+1	twin set 1
248	76	319	52	−1	twin set 2
71	58	119	47	−1	twin set 3
36	81	120	33	−1	twin set 1
79	83	353	28	−1	twin set 2
130	89	40	4	−1	

magnitude of dip of the fault, azimuth and plunge of the striation (slip vector) and the displacement sense (see Tables 1 and 3).

3.2. Fault-striae datum characteristic variables

The graphical right-dihedra stress construction is made for each fault (Fig. 4). The stereographic procedure consists plotting the fault plane. Then line B perpendicular to the striation vector is determined within the fault plane. The conjugate nodal plane going through the fault plane normal and line B is constructed. The sphere is divided into two compression and two extension dihedras, which are displayed in a stereonet following Angelier and Mechler (1977). The solution is sampled on a dense grid to obtain binary dynamic attributes. Compression dihedra generate capable stress tensors; extensional dihedra generate non-capable stress tensors. In this way each fault is characterised by a string of variables referring to its compatibility (capable or non-capable) with the grid (Table 4a). The right-dihedra construction itself indicates the dichotomy of stress states, which are capable and incapable of causing observed twinning (faulting). That is why no special right-dihedra constructions are made for untwinned *e*-planes. Such a construction would result in a much broader map of incompatible stress states, obscuring the subsequent cluster analysis.

3.3. Similarity coefficients matrix

When each fault is characterised by the string of variables, all possible fault pairs are matched (Table 4b). The similarity between fault i and fault j is determined from the comparison of their variables. The most commonly used simple matching coefficient S_{ij} assigns the same weight on a_{ij} and d_{ij}, following Everitt (1980):

$$S_{ij} = (a_{ij} + d_{ij})/n, \tag{2}$$

where a_{ij} is the number of grid nodes where compressional right-dihedra solutions of both faults overlap, d_{ij} is the number of grid nodes which are not overlapped by either of both compressional right-dihedra solutions and n is the number of grid nodes.

The quantities a_{ij} and d_{ij} are descriptors of fault *closeness* that have the equal weight, i.e. *failing to fit* has equal value to *fitting*. The similarity coefficient S_{ij} varies from 0 (completely unrelated faults) to 1 (completely similar faults).

The similarity coefficients of fault pairs affect the later fault separation into dynamically-homogeneous subsets (Table 4b; Fig. 5).

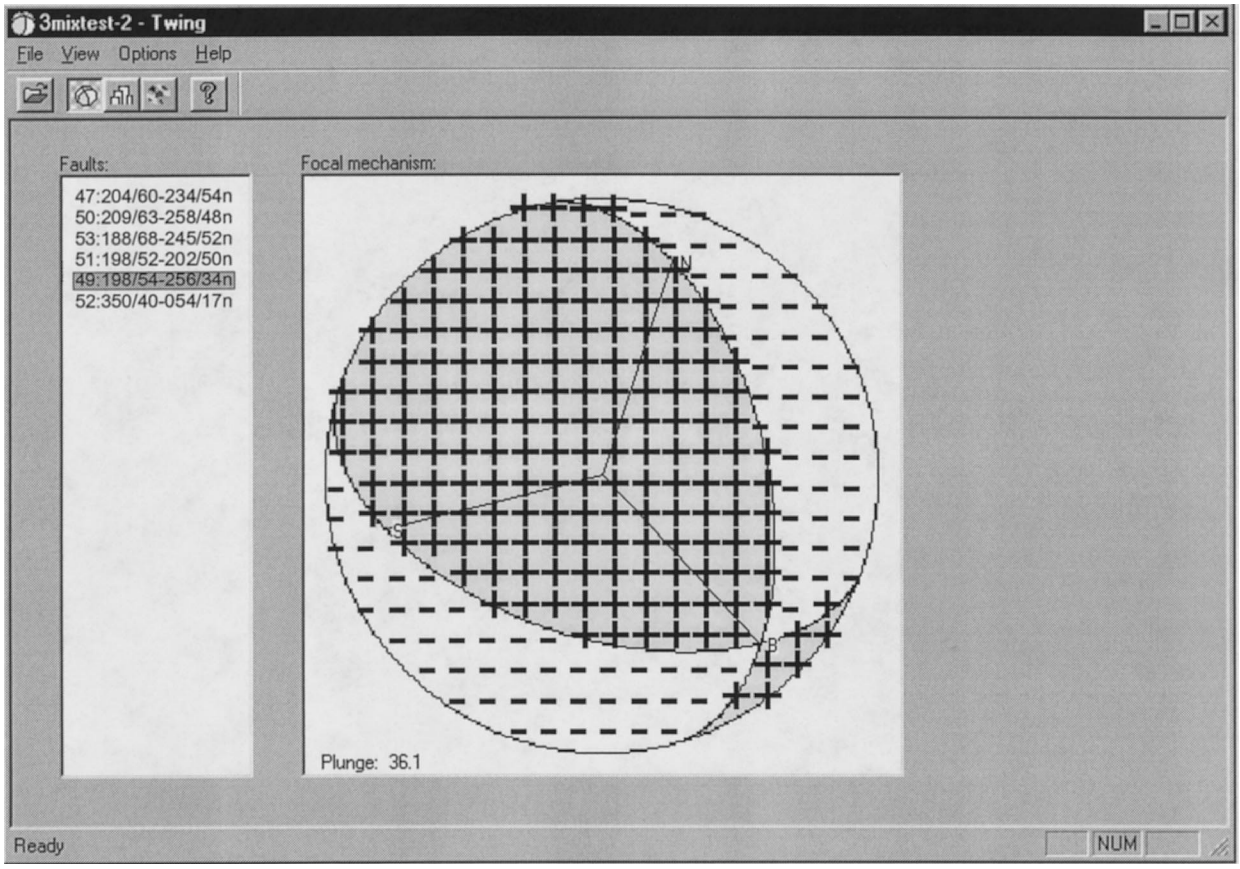

Fig. 4. Assignment of descriptive attributes to highlighted fault No. 49 on the basis of the right-dihedra solution (focal mechanism) matched against the grid. The fault-striae datum comprises dip direction and dip of the fault plane, trend and plunge of the striae and indication of the displacement (*n*—normal fault, *s*—sinistral strike-slip fault). The fault is given a string of binary attributes used for the later comparison of faults (Table 4a). +: grid point fits the compression dihedra projection. −: grid point does not fit the compression dihedra solution. Striation plunge correction (Plunge) of the field measurement mistake, in the case when measured striation does not lie on a great circle of the measured fault plane, is shown in the lower left corner. N—fault plane normal, S—striation, B—vector perpendicular to the striation vector and lying in the fault plane. Figure shows the snap shot of the software TWING after the separation of the data set III from *3mixtest* file (Table 1).

Table 4
(a) Defining binary dynamic attributes to each fault on the basis of the correlation of the compression dihedra with grid nodes. The string of binary attributes assigned to each fault is later used for the similarity coefficient computation. (b) Fault pairs characterised by their similarity coefficient S_{ij} calculated from and a_{ij}, d_{ij} and n [Eq. (2)]; where a_{ij} is the number of common grid squares where right-dihedra solutions of both faults overlap, d_{ij} is the number of common grid squares which are not overlapped by either of both right-dihedra solutions and n is the number of grid squares

	Square 1	Square 2	Square 3	Square 4	Square 5	Square 6	Square 7
(a)							
Fault 1	+	−	+	+	−	−	−
Fault 2	+	+	+	+	−	−	+
Fault 3	−	−	+	−	+	+	+
Fault 4	−	−	−	−	+	+	+
(b)							
Fault pair	1&2	$a_{12}=3$	$d_{12}=2$	$n=7$	$S_{ij}=0.6100$		
Fault pair	1&3	$a_{13}=1$	$d_{13}=1$	$n=7$	$S_{ij}=0.1700$		
Fault pair	1&4	$a_{14}=0$	$d_{14}=1$	$n=7$	$S_{ij}=0.0066$		
Fault pair	2&3	etc.					

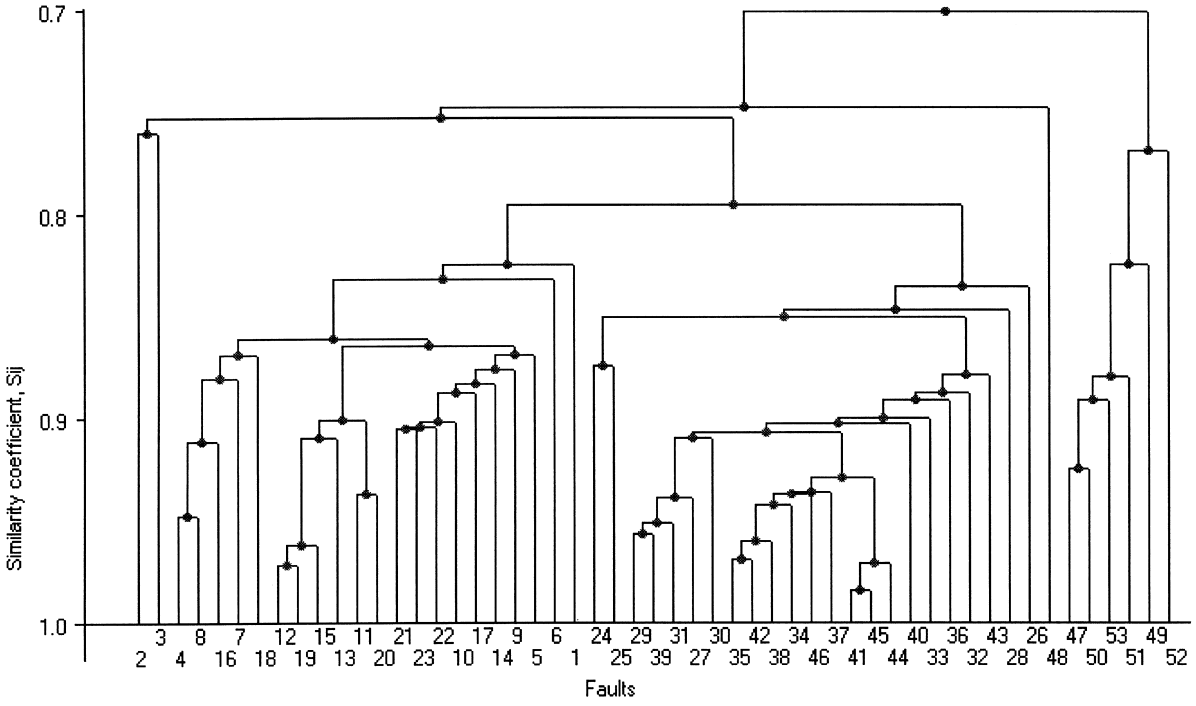

Fig. 5. Fault separation of the data set *3mixtest* from Table 1. The fault groupings in the dendrogram are made by cluster analysis. Three first-order branches are related to data sets I, II and III (Fig. 2) mixed in a *3mixtest* file (Table 1). Note that due to the less limiting constraints imposed by the right-dihedra solution, because of its design for the disperse calcite twin data, the separation cuts deeper inside the three monophase data sets. It results in separated data sets I and III missing faults Nos. 3 and 4 and No. 48, respectively.

3.4. Clustering and separation

A hierarchical clustering, specifically the agglomerative technique of cluster analysis called the *single link method* was chosen from the variety of available methods (see Everitt, 1980). It begins with the similarity matrix between the entities and ends with a dendrogram showing the successive fusions of individuals that results in the stage in which all individuals are grouped. At each stage the method unites individuals according to the distance between their nearest members. The distance between groups is defined as the distance between their closest members. Readers interested in detailed discussion of the *single link clustering* are referred to Everitt (1980).

Fig. 5 shows the sequence of fusion of our data from Table 1 governed by the ranked similarity coefficients from their similarity matrix. The sequence of fusions is recorded graphically in the dendrogram. The first-order branches of the tree indicate the membership of the dominant fault subsets (Fig. 5). Each merger point in the dendrogram is the point of optional data separation. Thus, the first-order branches can be separated into fault-striae subsets, e.g. a subset in Fig. 4. In as much as the sequence of mergers ends in a merger of all data, the separation has to be made downward until a further separation of outliers from the first-order branches does not result in a different calculated stress solution.

3.5. Composite right-dihedra solution

The composite right-dihedra solution is constructed for each separated fault-striae subset. The solution either yields the principal stresses for the monophase subset or indicates that a subset is not monophase.

The graphical right-dihedra stress solution is determined for each fault of a subset (Fig. 4). All solutions are overlaid and matched against a grid. Each grid node counts the amount of overlaps with compression dihedras of each solution projected on the stereonet. The result is a contour map of the stereonet (Figs. 6 and 7). Areas with 0 value indicate the solution for the minimum compressive stress σ_3 distribution. Areas with maximum value, equal to the amount of faults in the data set, indicate the solution for the maximum compressive stress σ_1 distribution. The composite right-dihedra solution forms a control of the separation for the fault-striae data. When the number of the overlays in the contoured maximum is less than the total number of the faults in the data set, the separated data set is not a dynamically-homogeneous fault set. In this case the screening process has to be repeated and a separation has to be made at a higher similarity coefficient S_{ij} level.

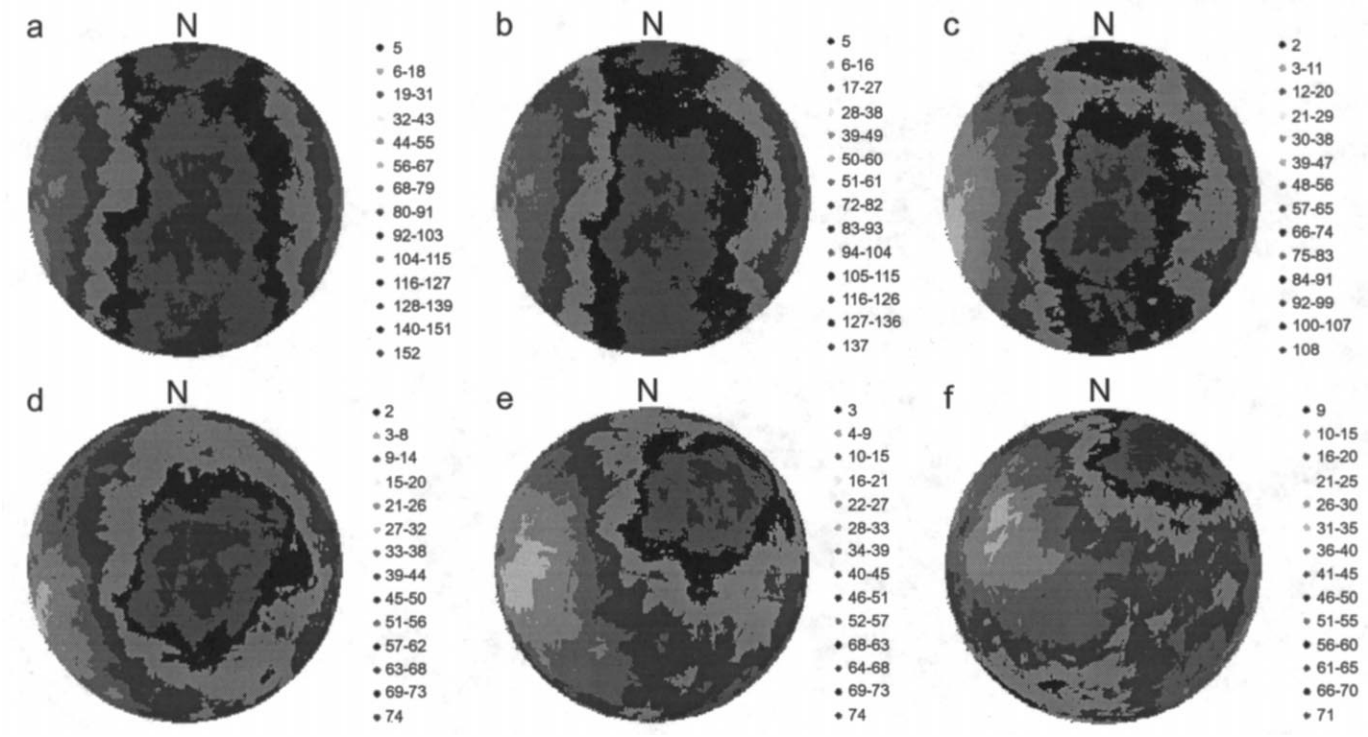

Fig. 6. Attempts to reproduce the stress state used by Laurent (Table 5) when he created the experimental calcite twin data set *Buxy 00* (Tables 2 and 3) by our software TWING. The graphical output of the calculation is shown for: (a) the whole *Buxy 00* data set; (b) the first 200 faults of the *Buxy 00* data set; (c) the first 150 faults of the *Buxy 00* data set; (d) the first 100 faults of the *Buxy 00* data set; (e) the *Buxy 30* data set = first 100 faults of the *Buxy 00* data set rotated 30°; (f) the *Buxy 60* data set = first 100 faults of the *Buxy 00* data set rotated 60°. Trend/plunge of the rotation axis is 114/00. Calculated orientations of principal stress axes (trend/plunge) and their stress ratio are: (a) 193/71, 344/17, 077/09, 0.231; (b) 183/80, 323/08, 054/07, 0.204; (c) 189/77, 326/10, 057/08, 0.190; (d) 061/83, 325/01, 235/07, 0.075; (e) 035/66, 138/06, 230/23, 0.110; (f) 033/31, 131/13, 241/55, 0.265. Note that the reduction of the data (diagrams b, c, d) did not affect the resulting stress and that all results are similar to real stresses (Table 5).

This constraint can fail in the case of the natural calcite twin data, which display a broad range of orientations (Figs. 6 and 7). In such a case, the separation has to be made downward until subsets result in similar stress solutions. An example of how the natural twin data scatter affects the resulting stress calculation is best shown in the case of the experimentally made data set *Buxy 00* provided by Laurent (Tables 2 and 3). The estimated amount of outliers (twins made prior to experiment) is 0.5% (Laurent, 1998, personal communication). However, the minimum (5) and maximum (152) values in Fig. 6(a) indicate that the number of 'outliers' is larger, i.e. formed by real outliers plus data belonging to the data set.

When the initial test indicates that the separated cluster forms the dynamically-homogeneous fault-striae set, i.e. the fault population controlled by the single stress event, the ratio of the stress magnitudes is calculated. At the start of this calculation, each grid node on the stereonet is defined by the unit vector oriented from the centre towards the node, defined by its directional cosines (l, m, n). The number of overlays counted by grid node is used to multiply the length of the unit vector, i.e. the amount of overlaps defines the number of identically oriented vectors. Thus, the contoured composite right-dihedra solution was transformed to the set of vectors of various lengths, all starting in the centre of the sphere represented by the stereonet. The orientation matrix of this vector set is calculated following Scheidegger (1965):

$$\mathbf{A} = \begin{bmatrix} \Sigma l_i^2 & \Sigma l_i m_i & \Sigma l_i n_i \\ \Sigma l_i m_i & \Sigma m_i^2 & \Sigma m_i n_i \\ \Sigma l_i n_i & \Sigma m_i n_i & \Sigma n_i^2 \end{bmatrix} \tag{3}$$

The shape of the ellipsoid representing this orientation tensor is defined by the eigenvalues (Pfiffner and Burkhard, 1987; Wallbrecher and Fritz, 1989; Wallbrecher et al., 1996) δ_1, δ_2 and δ_3, where $\delta_1 \geq \delta_2 \geq \delta_3$. Thus their ratio R represents the ratio of magnitudes of the principal stresses:

$$R = (\delta_2 - \delta_3)/(\delta_1 - \delta_3) \tag{4}$$

that varies between 0 and 1.

When the stress ratio is calculated, the areas of minimum and maximum are separated from the composite right-dihedra solution. As with the case of the composite solution, each grid node of the right-dihedra

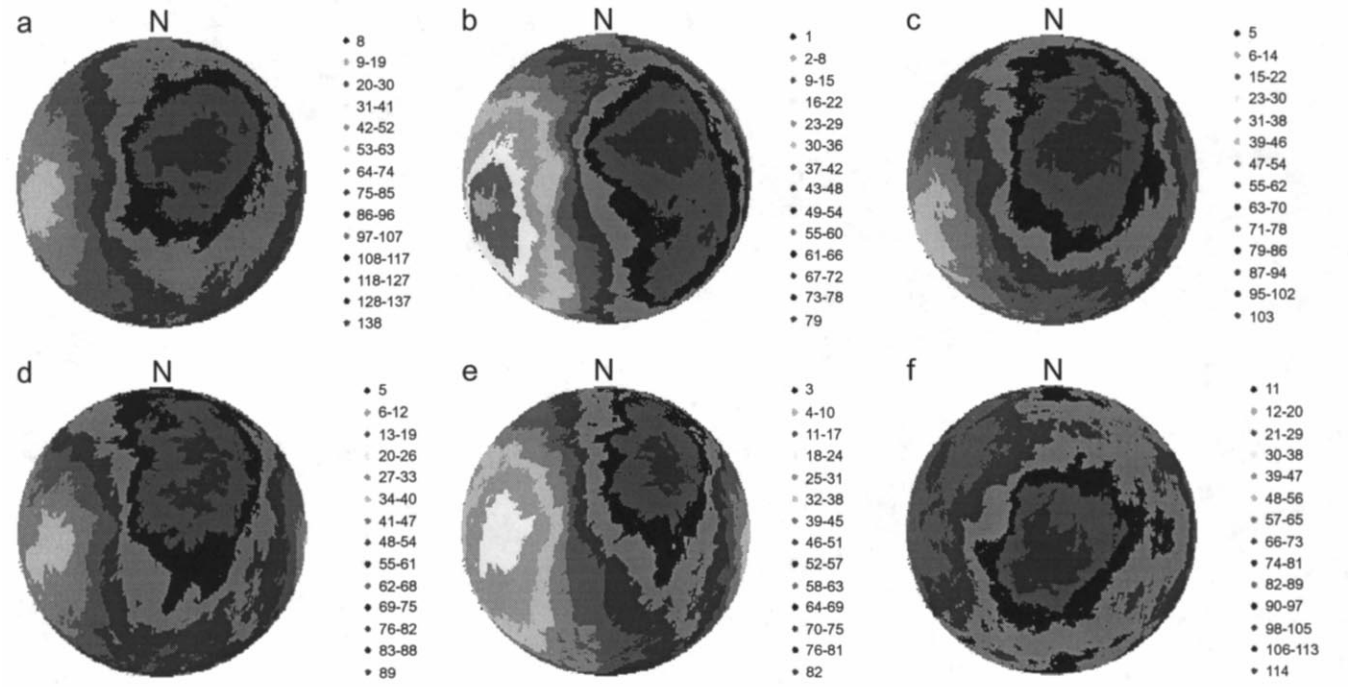

Fig. 7. Examples of separation results from data sets *Buxy 00-30mix*, *Buxy 00-60mix* and *Buxy 00-90mix* (files contain a mixture of the first 100 faults of the *Buxy 00* data set with the same data set, but rotated about an indicated amount). Diagrams show the composite right-dihedra solutions calculated from subsets separated from: (a, b) *Buxy 00-30mix*; (c, d, e) *Buxy 00-60mix*; and (f) *Buxy 00-90mix*. Calculated orientations of principal stress axes (trend/plunge) and their stress ratio are: (a) 062/76, 316/00, 225/13, 0.107; (b) 060/63, 322/04, 230/27, 0.207; (c) 054/71, 321/01, 231/19, 0.094; (d) 019/55, 139/19, 240/28, 0.168; (e) 038/50, 140/10, 238/39, 0.216; (f) 193/72, 326/11, 058/13, 0.074. (a–c, e and f) Final results of the separation. (d) and (e) Second last and last step downward in the dendrogram during the separation. Note, that all final results are similar to real stresses listed in (Table 5).

$$\mathbf{A} = \begin{bmatrix} \Sigma(l_{xi}^2 - l_{zi}^2) & \Sigma(l_{xi}m_{xi} - l_{zi}m_{zi}) & \Sigma(l_{xi}n_{xi} - l_{zi}n_{zi}) \\ \Sigma(m_{xi}l_{xi} - m_{zi}l_{zi}) & \Sigma(m_{xi}^2 - m_{zi}^2) & \Sigma(m_{xi}n_{xi} - m_{zi}n_{zi}) \\ \Sigma(n_{xi}l_{xi} - n_{zi}l_{zi}) & \Sigma(n_{xi}m_{xi} - n_{zi}m_{zi}) & \Sigma(n_{xi}^2 - n_{zi}^2) \end{bmatrix} \quad (5)$$

is defined by the unit vector starting in the centre of the sphere represented by the stereonet. The geometry of this configuration is formed by two 'cones' of vectors defined by (l_{xi}, m_{xi}, n_{xi}) in the case of the maximum (compression) and by (l_{zi}, m_{zi}, n_{zi}) in the case of minimum (extension). The orientation matrix of this vector set is calculated by the approach for two mutually perpendicular sets, following Lisle (1989):

Table 5
Stresses related to files with experimental calcite twin data. File *Buxy 00* is the original data set made by Laurent (Table 2) under the stress described here. Data files *Buxy 30*, *60* and *90* were made by rotation. The trend/plunge of the rotation axis is 114/0. Angles of rotation are 30°, 60° and 90°. Stresses related to files *Buxy 30*, *60* and *90* were determined by the same rotation

File	σ_1 (trend/plunge)	σ_2 (trend/plunge)	σ_3 (trend/plunge)	R
Buxy 00	204/87	317/01	047/00	0.07
Buxy 30	024/63	135/10	230/27	0.07
Buxy 60	024/33	127/19	244/53	0.07
Buxy 90	024/03	115/23	294/67	0.07

The orientations of the principal stress axes are given by the eigenvectors. The stress inversion from the separated dynamically-homogeneous fault set is finished by the recalculation of direction cosines of the stress axes to the trend/plunge format (Figs. 6 and 7).

4. Method testing

The method is tested by three dynamically mixed fault-striae data sets, *3mixtest* (Table 1), made from synthetic calcite twin data (Fig. 2) generated by a simple algorithm. It is also tested by several files with two dynamically mixed fault-striae data sets, *Buxy 00-30mix*, *Buxy 00-60mix* and *Buxy 00-90mix*, which were compiled from twin data generated experimentally by Laurent (Fig. 3; Tables 2 and 3). Data sets from Table 1 are generated numerically to gain the 100% control on dynamically mixed sets, their stress states and the success of their separation. The data set from Tables 2 and 3 is generated from rock mechanics experiments

(Laurent, 1998, personal communication). A presence of the twin data prior to this experiment (0.05%) and the natural twin data scatter make the control slightly less precise. As discussed by Nemcok and Lisle (1995), the mixing of natural calcite twin data would not provide a reliable check of the separation method.

Fig. 5 shows the dendrogram made by the cluster analysis of the *3mixtest* data from Table 1. The separated subsets at the level 0.8 of the similarity coefficient S_{ij} are dynamically homogeneous; the first discarding faults Nos. 2 and 3, the second one removing none and the third one removing the fault No. 48. In spite of the minimal rejection of faults from homogeneous subsets, driven by the higher degree of freedom given by the probability properties of the right-dihedra solution in comparison with the method of Nemcok and Lisle (1995), the separation technique was capable of correct definition of dynamically homogeneous subsets. None of the resultant subsets is contaminated by members of the other subsets. The subsets are dynamically homogeneous and suitable for the monophase stress inversion.

Testing based on the experimentally derived data set *Buxy 00* (Tables 2 and 3; Fig. 3) was more complex. Compiled data sets which were used in dynamically-mixed tests (*Buxy 00-30mix*, *Buxy 00-60mix*, *Buxy 00-90mix*) were obtained by incremental rotation of *Buxy 00* and its addition to original *Buxy 00*. The trend and plunge of the rotation axis were 114° and 0°, respectively, angle of rotation was 30°, 60° and 90°. The stress state used for the experiment (Laurent, 1998, personal communication) and rotated stress states related to *Buxy 30*, *Buxy 60* and *Buxy 90* are listed in Table 5. The first test runs indicated that the natural scatter of the twin data does not have any influence on the calculated stress state (Fig. 6a–d). The rotation of data did not affect the calculated stress state (Fig. 6e and f). Separation tests indicate that resulting stress states determined for separated subsets fit the real stress states (Fig. 7; Table 5).

Separation tests indicate that the calcite twin data have to be treated differently from fault-striae data. In the case of the dynamically-mixed fault-striae data, the separation is realised when the composite right-dihedra solution results in the 0% data overlap area inside the extensional dihedra and the 100% data overlap area inside the compressional dihedra. This is a requirement that the subset is dynamically-homogeneous. In the case of the dynamically-mixed calcite twin data, the separation is realised when further separation downward in the dendrogram does not result in a distinct change in the calculated stress state.

The success of the separation depends, in general, on the difference between the right-dihedra solutions of the samples and the density of the matching grid nodes. In spite of the minimal rejection of faults from homogeneous subsets, driven by the higher degree of freedom given by the probability properties of the right-dihedra solution, the separation technique is capable of correct definition of dynamically homogeneous subsets. None of the resultant subsets is contaminated by members of the other subsets.

5. Conclusions

The proposed method pre-processes calcite twin and fault data to group them on the basis of their response to all possible orientations and magnitudes of applied stress. It appears that the method bypasses the generation of spurious average stress solutions caused by the search for the *best-fit stress tensor* that in turn influences the data separation into coherent dynamically homogeneous subsets.

Our method describes each fault by a string of variables, which is derived from the right-dihedra solution. These variables are dynamic attributes relating this fault to the compatible and incompatible stress tensors. Dynamic attributes are used in a calculation of the similarity coefficient matrix which quantifies degrees of similarity of the faults based on their response to multiple stress tensors.

The applied agglomerative cluster technique proved to be efficient in the successful separation of dynamically-homogeneous subsets by comparing the similarity coefficients of all fault pair combinations.

The suggested technique is not limited by any imposed constraint in its search for the homogeneous subsets. The utilised right-dihedra core of the method allows a less limited freedom in the search for fault similarities than the fully numerical method of Nemcok and Lisle (1995). This makes the method especially suitable for the analysis of the calcite twin data, but also keeps it suitable for the fault-striae data. The final right-dihedra solution is recalculated into *reduced stress tensor*.

The method is programmed in C++ language software for Windows 95, 98 and Windows NT.

Acknowledgements

The idea of the use of the orientation matrix was developed after discussions with Harald Fritz, Martin Burkhard, Rostislav Melichar and Eckart Wallbrecher. We are grateful to Lothar Ratschbacher and Franz Neubauer for financing of programming. The theoretical part of the work was carried out during MN's tenure of the Lise-Meitner FWF Post-Doctoral Research Fellowship in Salzburg. Philippe Laurent kindly provided the experimental calcite twin data. Blanka Sperner kindly provided the calcite defor-

mation software package and assistance in data conversions. The paper benefited from critical reviews by Jacques Angelier and Philippe Laurent and a friendly review by Steven Schamel.

References

Angelier, J., 1979. Determination of the mean principal directions of stresses for a given fault population. Tectonophysics 56, T17–T26.

Angelier, J., 1984. Tectonic analysis of fault slip data sets. Journal of Geophysical Research 89, 5835–5848.

Angelier, J., 1989. From orientation to magnitudes in paleostress determinations using fault slip data. Journal of Structural Geology 11, 37–50.

Angelier, J., 1990. Inversion of field data in fault tectonics to obtain the regional stress—III: A new rapid direct inversion by analytical means. Geophysical Journal International 103, 363–376.

Angelier, J., 1994. Fault slip analysis and palaeostress construction. In: Hancock, P.L (Ed.), Continental Deformation. Pergamon Press, Oxford, pp. 53–100.

Angelier, J., Manoussis, S., 1980. Classification automatique et distinction des phases superposées en tectonique de faille. Comptes Rendu de l'Académie des Sciences Paris 290, 651–654.

Angelier, J., Mechler, P., 1977. Sur une méthode graphique de récherche des contraintes principales également utilisable en tectonique et en seismologie: la methode des diédres droits. Bulletin de la Sociètè géologique France 19, 1309–1318.

Armijo, R., Carey, E., Cisternas, A., 1982. The inverse problem in microtectonics and the separation of tectonic phases. Tectonophysics 82, 145–160.

Bott, M.H.P., 1959. The mechanics of oblique-slip faulting. Geological Magazine 96, 109–117.

Burkhard, M., 1993. Calcite twins, their geometry, appearance and significance as stress–strain markers and indicators of tectonic regime: a review. Journal of Structural Geology 15, 351–368.

Carey, E., Brunier, B., 1974. Analyse théorique et numérique d'un modèle méchanique élémentaire appliqué à l'étude d'une population de failles . C. R. Hebd. Séances. Acad. Sci. Sér. D 279, 891–894.

Dietrich, D., Song, H., 1984. Calcite fabrics in a natural shear environment, the Helvetic nappes of western Switzerland. Journal of Structural Geology 6, 19–32.

Dupin, J.M., Sassi, W., Angelier, J., 1993. Homogeneous stress hypothesis and actual fault slip: a distinct element analysis. Journal of Structural Geology 15, 1033–1043.

Etchecopar, A., 1984. Etude des états de contraintes sur tectonique cassante et simulation de déformations plastiques (approche mathématique). Thesis, University Montpellier, pp. 1–270.

Etchecopar, A., Vasseur, G., Daignières, M., 1981. An inverse problem in microtectonics for the determination of stress tensors from fault striation analysis. Journal of Structural Geology 3, 51–65.

Everitt, B., 1980. Cluster Analysis, 2nd ed. Heinemann, Oxford.

Galindo-Zaldivar, J., Gonzales-Lodeiro, F., 1988. Faulting phase differentiation by means of computer search on a grid pattern. Annales Tectonicae 2, 90–97.

Gephart, J.W., 1990. FMSI: a FORTRAN program for inverting fault/slickenside and earthquake focal mechanism data to obtain the regional stress tensor. Computers and Geosciences 16, 953–989.

Gephart, J.W., Forsyth, D.W., 1984. An improved method for determining the regional stress tensor using earthquake focal mechanism data: Application to the San Fernando earthquake sequence. Journal of Geophysical Research 89, 9305–9320.

Hardcastle, K.C., Hills, L.S., 1991. BRUTE3 and SELECT: Quickbasic 4 programs for determination of stress tensor configurations and separation of heterogeneous populations of fault-slip data. Computers and Geosciences 17, 23–43.

Huang, Q., 1988. Computer-based method to separate heterogeneous sets of fault-slip data into sub-sets. Journal of Structural Geology 10, 297–299.

Kleinspehn, K., Pershing, J., Teyssier, C., 1989. Palaeostress stratigraphy: a new technique for analysing tectonic control on sedimentary-basin subsidence. Geology 17, 253–257.

Lacombe, O., Laurent, P., 1996. Determination of deviatoric stress tensors based on inversion of calcite twin data from experimentally deformed monophase samples: preliminary results. Tectonophysics 255, 189–202.

Laurent, P., 1984. Les macles de la calcite en tectonique: nouvelles méthodes dynamiques et premières applications. Thesis, University Montpellier, pp. 1–324.

Laurent, P., Bernard, P., Vasseur, G., Etchecopar, A., 1981. Stress tensor determination from the study of e twins in calcite: a linear programming method. Tectonophysics 78, 651–660.

Laurent, P., Tourneret, C., Laborde, O., 1990. Determining deviatoric stress tensors from calcite twins. Application to monophased synthetic and natural polycrystals. Tectonics 9, 379–389.

Lisle, R.J., 1989. The statistical analysis of orthogonal orientation data. Journal of Geology 97, 360–364.

Michael, A.J., 1984. Determination of stress from slip data: faults and folds. Journal of Geophysical Research 89, 11517–11526.

Mügge, O., 1883. Beiträge zur Kenntnis der Strukturflächen des Kalkspathes. Neues Jahrbuch für Mineralogie 1, 32–54.

Nemcok, M., Lisle, R.J., 1995. A stress inversion procedure for polyphase fault/slip data sets. Journal of Structural Geology 17, 1445–1453.

Nissen, H.U., 1964. Dynamic and kinematic analysis of deformed crinoid stems in a quartz graywacke. Journal of Geology 72, 346–368.

Pfiffner, O.A., Burkhard, M., 1987. Determination of paleo-stress axes orientations from fault, twin and earthquake data. Annales Tectonicae 1, 48–57.

Pollard, D.D., Salitzer, S.D., Rubin, A.M., 1993. Stress inversion methods: are they based on faulty assumptions? Journal of Structural Geology 15, 1045–1054.

Reches, Z., 1987. Determination of the tectonic stress tensor from slip along faults that obey the Coulomb yield condition. Tectonics 6, 849–861.

Rose, G., 1868. Ueber die Kalkspath vorkommenden hohlen Kanäle. Abh. Königl. Akad. Wiss. Berlin 23, 57–79.

Scheidegger, A.E., 1965. On the statistics of the orientation of bedding planes, grain axes, and similar sedimentological data. US Geological Survey Professional Paper 525-C, pp. 164–167.

Simón-Gómez, J.L., 1986. Analysis of a gradual change in stress regime (example from the eastern Iberian Chain). Tectonophysics 124, 37–53.

Spang, J.H., 1972. Numerical method for dynamic analysis of calcite twin lamellae. Geological Society of America Bulletin 83, 467–472.

Sperner, B., Ratschbacher, L., 1994. A Turbo Pascal program package for graphical presentation and stress analysis of calcite deformation. Zeitschrift der Deutschen Geologishen Gesells Chaft 145, 414–423.

Turner, F.J., 1953. Nature and dynamic interpretation of deformation lamellae in calcite of three marbles. American Journal of Science 251, 276–298.

Turner, F.J., 1962. "Compression" and "tension" axes deducted from {0112} twinning in calcite. Journal of Geophysical Research 67, 1660.

Wallace, R.E., 1951. Geometry of shearing stress and relation to faulting. Journal of Geology 59, 118–130.

Wallbrecher, E., Fritz, H., 1989. Quantitative evaluation of the shape factor and the orientation of paleo-stress ellipsoid from the distribution of slickenside striations. Annales Tectonicae 3, 110–122.

Wallbrecher, E., Fritz, H., Unzog, W., 1996. Estimation of the shape factor of a palaeostress ellipsoid by comparison with theoretical slickenline patterns and application of an eigenvalue method. Tectonophysics 255, 177–187.

Weiss, L.E., 1954. A study of tectonic style: Structural investigation of a marble quartzite complex in southern California. University of California Publications in Geological Sciences 30, 1–102.

Wenk, H.R., Barber, D.J., Reeder, R.J., 1983. Microstructures in carbonates. In: Reeder R.J (Ed.), Carbonates: Mineralogy and Chemistry, vol. 11. Rev. Meiner. Miner. Soc. Am, pp. 301–367.

Will, T.M., Powell, R., 1991. A robust approach to the calculation of paleostress fields from fault plane data. Journal of Structural Geology 13, 813–821.